Vol. 13, Sp. Issue 03 July: 2025
ISSN(P) 2347-5404 ISSN(O)2320 771X

The Size, Complexity of Molecules and Electronic Properties of Graphene

LAL MOHAN MAHATO
Research Scholar,
Department of Physics
C.C.S. University, Meerut, UP

DR. LAL SINGH
Research Supervisor,
Department of Physics
C.C.S. University, Meerut, UP

1. Introduction

Theoretical studies of electronic properties of graphene-based system involve to a large extent heavy calculations. The incredible progress of computers, high performance computing in particular, has made it possible to perform such studies using very accurate quantum mechanical methods.

The size and complexity of molecules, polymers or unit cells of crystals that can be treated with ab initio quantum chemistry or VASP methods have increased dramatically. Today we are on a routine base performing ab initio calculations of molecules or unit cells with hundreds of atoms and thousands of electrons. Such studies deal with ground state properties which forms the basis for the understanding of material properties. However, when dealing with properties that are directly related to electronic application, properties such as mobility and conductivity, it is considerably more difficult to obtain realistic results for large systems. Partially, this is due to the fact that we lack some important information concerning the electronic device for example, the exact nature of the contacts or knowledge about defects in the material. It is also considerably more difficult to calculate quantities that depends on defects or a detailed interactions at constant interfaces.

The work in this thesis is based on calculations ab initio level but also using parametrised Hamiltonian of contact and conductance properties. These methods are introduced in chapter 2 below and also presented at a more detailed level in the articles.

In all the DFT calculations presented in this thesis in chapter 3 and 4 the Vienna ab initio simulation package code VASP [1-3] has been used. It offers periodic boundary conditions on super-cells. This package provides both LDA and GGA exchange-correlation energy functional. For the studied molecular crystals the PW91 version of the GGA was chosen.

In this thesis, we will investigate four graphene [4-6] based systems:
1. Single Layer Graphene
2.Bilayer Graphene
3.Graphene Nanoribbons
4.Bilayer Graphene Nanoribbons

For each system, we will discuss the peculiar geometry of each system and calculate their electronic dispersion relations and wave functions using the tight binding approximation and the overlap integrals calculated by DFT. This is the subject of the present chapter.

The Hamiltonian for all systems considered is calculated using the tight binding approximation [7] which is written in second quantized notation and momentum (**k**) space by

$$H = \sum_{i,j,k} t_{ij} e^{i\mathbf{k}.\delta_{ij}} \alpha_i^{\dagger}(\mathbf{k}) \alpha_j(\mathbf{k}) \quad (1)$$

Where i and j denote the i^{th} and j^{th} atoms in the unit cell, t_{ij} is the overlap integral of the wavefunctions of the i^{th} and j^{th} atoms in the unit cell, and $\hat{\delta}_{ij}$ is the vector between those atoms. This is the most general form of a tight-binding Hamiltonian, where all the physics of the system is captured by the phase factors and overlap integrals. The overlap integrals can be calculated by density functional theory [8], and can be confirmed experimentally by numerous methods. The exact value of the coupling constants in graphene is by now means a closed topic. Even the most important quantity– the first nearest neighbors overlap integral–is not firmly agreed upon.

Nevertheless, only rough values are required for this thesis. Indeed, all overlap integrals shall be normalized by the first nearest neighbor overlap integral, and so only the approximate ratio of different constants will be required. All values used shall be consistent with the majority of the literature, which shall also be the justification for their use.

Usually only the vastly dominant first nearest neighbors are included in the calculations, unless the second nearest neighbors are particularly relevant. The value of the first nearest neighbor coupling is given by t ≈ 3eV. The second nearest neighbor overlap integral is given by t' ≈ 0.01eV ≈ t/30. The interlayer coupling constants for layered systems [9-12] will be introduced below.

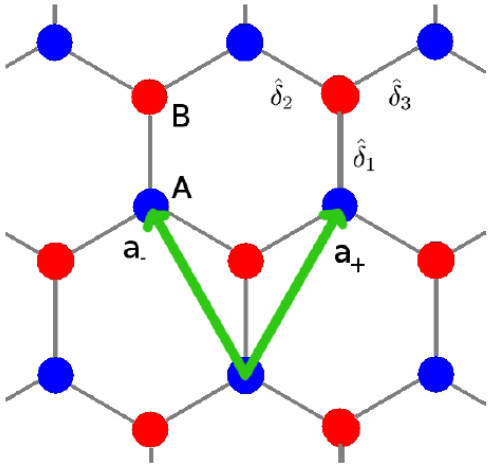

Figure 1: Single layer graphene contains two atoms per unit cell, generally denoted by A and B. The first nearest neighbour vectors and shown ($\hat{\delta}_i$), as well as the lattice vectors ($a_{\pm}$). The electronic structure is investigated via the tight binding approximation.

2. Single Layer Graphene (SLG)

Single layer graphene is the basic building block of all the subsystems encountered in this thesis. Graphene is a two-dimensional honeycomb lattice of carbon atoms. A slab of single layer graphene is shown in figure 3.1. As can be seen in the figure, there are two atoms in the unit cell denoted A and B. There are also three nearest neighbour vectors which are

$\hat{\delta}_1 = (0, b)$

$\hat{\delta}_2 = \left(\frac{\sqrt{3}b}{2}, -\frac{b}{2}\right)$ (2)

$\hat{\delta}_3 = \left(-\frac{\sqrt{3}b}{2}, -\frac{b}{2}\right)$

Where b = 1.42Å is the first nearest neighbour separation. This will be treated as the intrinsic length scale throughout the thesis, and so all lengths will be normalized by it. And the two lattice vectors are given by $\hat{\delta}_1 - \hat{\delta}_2$ and $\hat{\delta}_1 - \hat{\delta}_3$,
giving

$a_1 = \left(-\frac{\sqrt{3}b}{2}, \frac{3b}{2}\right)$ (3)

$a_2 = \left(\frac{\sqrt{3}b}{2}, \frac{3b}{2}\right)$.

Using Bloch's theorem and the tight binding approximation one can construct the 2D electronic dispersion for single layer graphene.

3. Full Energy Description

The original formulation of the electronic properties of SLG was calculated by P.R. Wallace in 1947 [10]. Whilst he didn't have graphene in mind as a material in its own right, Wallace used the single layer formulism to determine the electronic properties of bulk 3D graphite. For SLG with non-zero nearest neighbour hopping only, the matrix elements are given by

$${}_A\langle k|H|k\rangle_B = \frac{-t}{N}\sum_{R,R',R''}\left(e^{-ik.(R'-R'')}(\langle R'|R\rangle\langle R+\hat{\delta}_1|R''\rangle + \langle R'|R\rangle\langle R+\hat{\delta}_1-a_1|R''\rangle + \langle R'|R\rangle\langle R+\hat{\delta}_1-a_2|R''\rangle)\right)$$

$$= \frac{-t}{N}\sum_{R,R',R''}\left(e^{-ik.(R'-R'')}(\delta_{R'},R^{\delta}_{R+\hat{\delta}_1,R''} + \delta_{R'}R^{\delta}_{R+\hat{\delta}_1-a_1,}R'' + \delta_{R',R}\delta_{R+\hat{\delta}_1-a_2,R''}\right) (4)$$

$$= \frac{-t}{N}\sum_{R}\left(e^{-ik.(-\hat{\delta}_1)} + e^{-ik.(-\hat{\delta}_1-a_1)} + e^{-ik.(-\hat{\delta}_1-a_2)}\right)$$

$$= -te^{-ik.\hat{\delta}_1}(1+e^{ik.a_+}+e^{ik.a_-})$$

And

${}_B\langle k|H|k\rangle_A = {}_A\langle k|H|k\rangle_B^*$ (5)

The overlap of the atomic orbitals of neighboring sites in graphene will be the unit of energy by which all other energy values in this thesis will be normalized. The value of t in graphene is agreed to be t ≈ 3.0eV. The next nearest neighbours can easily be incorporated into the formalism in a similar manner, giving a Hamiltonian matrix of

$$H = \begin{pmatrix} t'H_{11}(\boldsymbol{k}) & t'H_{12}(\boldsymbol{k}) \\ tH_{12}(\boldsymbol{k}) & tH_{11}(\boldsymbol{k}) \end{pmatrix} (6)$$

Where

$$H_{12}(\mathbf{k}) = -e^{ik.\hat{\delta}_1}\left(1+e^{ik.a_+}+e^{ik.a_-}\right) (7)$$

And

$$H_{11}(\mathbf{k}) = \sqrt{3-|H_{12}(\boldsymbol{k})|^2} (8)$$

With t' ≈ t/30. The energy eigenvalues for this system are readily solved as

$E_S(\mathbf{k}) = t' H_{11}(\mathbf{k}) + st|H_{12}(\mathbf{k})|$(9)

Where s = ±1. We will define the special case where next nearest neighbor coupling is neglected (i.e. t' = 0) as

$$\epsilon_s(\mathbf{k}) = st|H_{12}(\mathbf{k})|^2 = st\sqrt{1+4\cos(k_x\sqrt{3}b/2)\cos(k_y/2)+4\cos^2(k_y/2)}$$ (10)

The wavefunctions are then easily obtained (and are identical for zero and non-zero t'), and given by

$$\psi(\mathbf{k}) = \frac{1}{\sqrt{2}}\begin{pmatrix} stH_{12}^*(\boldsymbol{k})/\epsilon_s(\boldsymbol{k}) \\ 1 \end{pmatrix} (11)$$

Which, by de-Moivres theorem, can be expressed as

$$\psi(\mathbf{k}) = \frac{1}{\sqrt{2}}\begin{pmatrix} ste^{i\phi(\boldsymbol{k})} \\ 1 \end{pmatrix} (12)$$

Where $\phi(\mathbf{k}) = \tan^{-1}(\Im H_{12}(\mathbf{k})/\Re H_{12}(\mathbf{k}))$.

4. Low Energy Approximation

The energy dispersion curve is given by

$\epsilon_s(k) = st|H_{12}(k)|^2 =$

st$\sqrt{1 + 4\,cos\,(k_x\,\sqrt{3}b/2)\cos(k_y/2) + 4\,cos^2(k_y/2)}$ (13)

Whose zeroes can be solved by

$\epsilon_s(\mathrm{k})^2 = \mathrm{t}^2(1 + 4\cos\left(k_x\,\sqrt{3}b/2\right)\cos(k_y/2)\ + 4\,cos^2\,(k_y/2)) = 0$ (14)

There are two inequivalent points that give zero energy, which are usually called the K-points or charge neutrality points. They are **K**, **K'** = $\left(\pm\,\frac{4\,\pi}{3\,\sqrt{3}}\,,0\right)$. Expanding around one of these points, we obtain a greatly simplified Hamiltonian matrix. To do this, we will proceed as follows: near the K-point, the momentum is given by **K** = $(K_x + \Delta_x, \Delta_y)$ (since K_y = 0). The Hamiltonian near the K-points then, is given by (in terms of the nearest neighbor vectors $\hat{\delta}_i$):

$-\mathrm{H}_{12}(\mathrm{k}) = e^{-i\Delta_y} + 2\,Cos\,(\frac{\sqrt{3}}{2}\,(K_x + \Delta_x))e^{i\Delta_y/2}$

$\approx 1 - i\Delta_y + 2\cos\,(\frac{2\pi}{3} + \frac{\sqrt{3}}{2}\,\Delta_x)\,(1 + i\,\frac{\Delta_y}{2})$

$= 1 - i\Delta_y + 2(1 + i\,\frac{\Delta_y}{2})\,(-\frac{1}{2}\cos\frac{\sqrt{3}}{2}\,\Delta_x) - \frac{\sqrt{3}}{2}\sin\,(\frac{\sqrt{3}}{2}\,\Delta_x))$ (15)

$= 1 - i\Delta_y + (1 + i\,\frac{\Delta_y}{2})\,(-1 - \frac{3}{2}\,\Delta_x)$

$= 1 - i\Delta_y - 1 - \frac{3}{2}\Delta_x - \,i\,\frac{1}{2}\Delta_y$

$= \frac{3}{2}\,(\Delta_x - i\Delta_y)$

If we define the group velocity to be $v_F = \frac{3t}{2}$, then we have

$H_K = v_F\begin{pmatrix} 0 & k_x - ik_y \\ k_x + ik_y & 0 \end{pmatrix}$ (16)

For **K** sufficiently small and near the K-points. This, in turn, leads to a very simple conical energy dispersion

$\epsilon_k(\mathbf{k}) = v_F|\mathbf{k}|$ (17)

The velocity v_F is $v_F \approx 10^6$ ms^{-1}. The wavefunctions are still given by the full energy form described in equation 1.12, but with

$\phi\,(\mathbf{k}) = \tan^{-1}\,(k_y/k_x)$.(18)

The two K points are equivalent unless there is coupling between them in which case a phase factor must be introduced. However, this will not be relevant for any of our subsequent work.

5. Bilayer Graphene (BLG)

Bilayer graphene is constructed by stacking two single layers on top of one another such that half the B atoms are directly above an A atom as shown in figure 2. This so-called 'Bernal' type stacking is the most common configuration for multilayer graphene [11,12]. There are three main types of interlayers coupling in BLG. The direct vertical A-B coupling, given by $\gamma_1 \approx$ t/10 ≈ 0.3eV. Because the coupling in this case is vertical, there is no induced phase factor in the k_x–k_y wavefunction. This term causes the two single layer subbands to split into two each, giving two valence bands and two conduction bands. The second dominant coupling term, $\gamma_2 \approx 0.12$eV, couples A–B sites between layers which are not directly above and below each other, leading to a phase factor which is associated with this term. This term is often called the 'trigonal' term. It causes the single valley K-points of SLG to split into three very small valley K-points, thus causing a 'trigonal warping' of the band structure. The third term, $\gamma_3 \approx 0.1$eV, couples *A–A* and *B–B* sites between layers, and also induces a phase factor since the sites are offsect in the *x–y* phane. This term causes a breaking of the *x–y* isotropy of the system, as will be seen in the dispersion curves below.

The Hamiltonian then, including next nearest neighbours (NNN), and the three interlayer coupling terms, is given by

$$H_{BLG} = \begin{pmatrix} t'H_{11} & tH_{12}^* & \gamma_3 H_{12} & \gamma_1 \\ tH_{12} & t'H_{11} & \gamma_2 H_{12}^* & \gamma_3 H_{12} \\ \gamma_3 H_{12}^* & \gamma_2 H_{12} & t'H_{11} & tH_{12}^* \\ \gamma_1 & \gamma_3 H_{12}^* & tH_{12} & t'H_{11} \end{pmatrix} \quad (19)$$

The eigenvalues and eigenvectors in the absence of γ_3 are readily solved. With γ_3 included however, the form of the solution is unwieldy. The eigenvalues in the simpler case are given by the (relatively) concise form

$$\epsilon_{\lambda,k} = t'(\epsilon_{SL}^2 - 3) + \lambda \sqrt{\epsilon_{SL}^2 + \frac{\gamma_{12}^+}{2} \mu\sqrt{\Gamma}} \quad (20)$$

Where

$$\Gamma = \epsilon_{SL}^2 \gamma_{12}^+ + \frac{(\gamma_{12}^+)^2}{4} + 2\gamma_1\gamma_2\epsilon_{SL}^2 \text{ Re } (H_{12}) \quad (21)$$

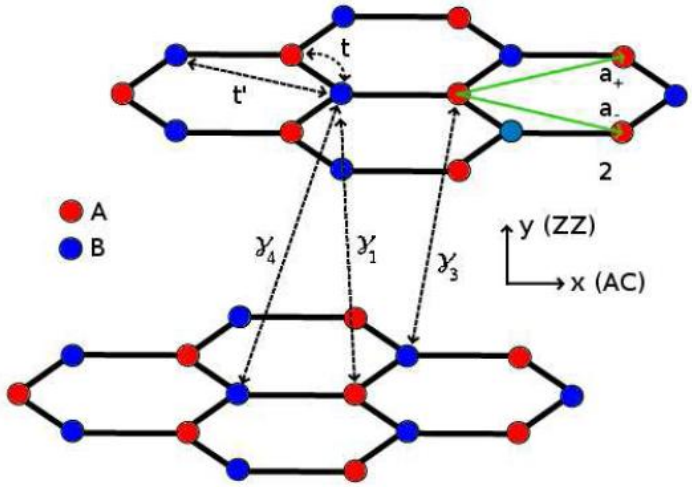

Figure 2: The three interlayer terms included in the BLG Hamiltonian, as well as the next nearest neighbour coupling term. γ_2 and γ_3 differ in that they connect, respectively, different and equivalent points in the SLG Brillouin Zone. Whilst γ_1 and γ_2 both represent coupling between different sites in the Brillouin zone, γ_1 is a directly vertical transition, and so the overlap of the wavefunctions is much larger ($\approx 3 \times$ larger)

And $\gamma_{12}^{\pm} = \gamma_2^2\epsilon_{SL}^2 \pm \gamma_1^2$, where λ, μ = ±1, ϵ_{SL} are the regular eigenvalues for the SLG system, and all coupling terms have been normalized by *t*. Form this result we see that there are two conduction bands and two valence bands which are confined above and below the line $\epsilon_{\lambda,\mu} - t'(\epsilon_{SL}^2 - 3)$. respectively.

The low energy part of the electronic dispersion curves are seen in figures 3 and 4. The NNN coupling has plunged the extrema below the Fermi energy. The effect of the dominant interlayer term γ_1 has caused a new pair of bands to emerge which, in this part of the spectrum, are separated from their pairs by an amount γ_1. The effect of γ_2 and γ_3 is much more subtle. The trigonal warping can be seen by the K-point pair in figure 4, and the γ_3 induced loss of isotropy between the two valleys can also be seen. Notice however, that the energy range of these effects is $\approx \gamma_2/1000$, which is extremely small.

Vol. 13, Sp. Issue 03 July: 2025
ISSN(P) 2347-5404 ISSN(O)2320 771X

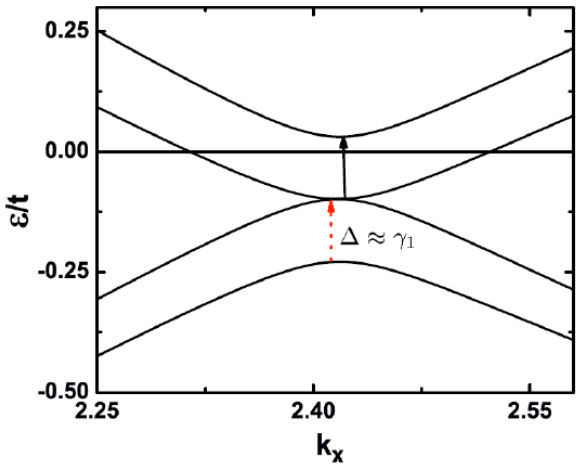

Figure 3: The k_x dependence of the band structure near the K/K' points with all coupling terms included. The two arrows show the approximately constant (at law energies) gap between similar bands.

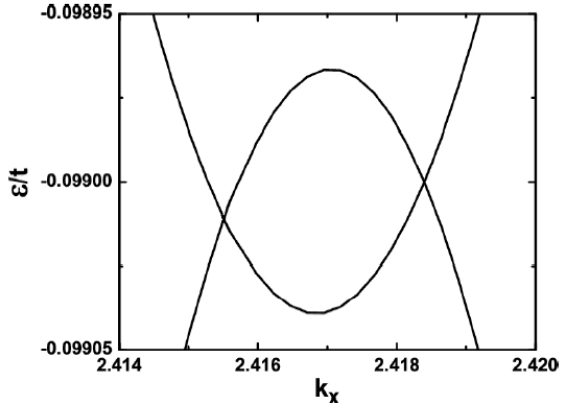

Figure 4: The k_x dependence of the two inner bands near the K/K' points zoomed right in to see the effects of γ_2 and γ_3. The NNN interaction has shifted these features well below the Fermi level. γ_2 causes the second dirac point to emerge, and γ_3 causes one of the two Dirac points to occur at a lower energy.

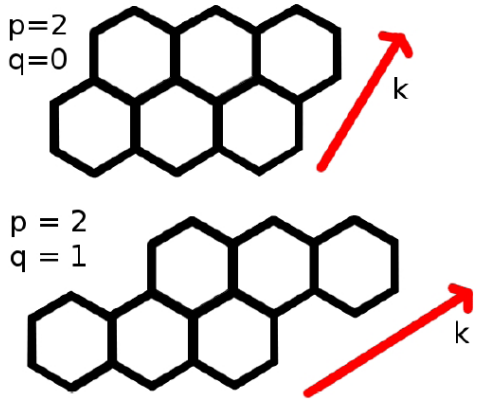

Figure 5: The two most typical GNRs are q = 0, corresponding to zig-zag ribbons, and q = 1, corresponding to armchair ribbons. The elegance of Ezawa's construction is the simplicity of constructing infinite ribbons by placing consecutive stacks of hexagon layers on top of each other, offset by q hexagons. The zig-zag and armchair edges can be readily seen. These are what determine the unique electronic properties of each class of ribbon. The index p essentially determines the width, and does not alter the electronic properties *as much* as q.

6. Graphene Nanoribbons (GNRs)

By cutting strips of single layer graphene, one can construct one dimensional graphene nanoribbons (GRRs). The electronic properties of GNRs [11-17] are both width dependent and chirality dependent. The construction of a GNR that we will use follows that introduced by Ezawa [18], and can be seen in figure 5. A GNR can be described by two indices <p,q>, where q determines the chirality, and $p + q$ is the number of hexagons placed side-by-side in the construction (see the figure). When constructed in this way, $q = 0$ defines a Zig-Zag (ZZ) edged GNR, and $q = 1$ defines and Armchair (AC) edged GNR. The chiral angle (θ_q) is defined as the angle between a zig-zag edge, and the axis direction of the ribbon. From this definition, $\theta_{ZZ} = 0$, and $\theta_{AC} = \pi/6$, and in general $\theta_q = \tan^{-1}\sqrt{3}/2q + 1)$.

The Hamiltonian for a GNR is given by

$$H_{GNR} = \begin{pmatrix} 0 & H_{AB} \\ H_{BA} & 0 \end{pmatrix} \quad (22)$$

Where the elements of H_{AB} are of from $t\, e^{ikb\cos(\theta_q+\phi_i)}$, and $H_{BA} = H_{AB}^{*}$. Here ϕ_i is the chiral angle of the unit vector that joins A and B such that

$\phi_i = \pi/6$

$\phi_2 = 5\pi/6$(23)

$\phi_3 = 3\pi/2$.

As an example, the Hamiltonian matrix for a <2,1> AC-GNR is

$$H_{<2,1>} = \begin{pmatrix} 0 & H_{AB}^{<2,1>} \\ H_{BA}^{<2,1>} & 0 \end{pmatrix} \quad (24)$$

Where

$$H_{BA}^{<2,1>} = \begin{pmatrix} e^{ikb\sqrt{3}/2} & e^{ikb} & 0 & 0 & 0 \\ e^{-ikb\sqrt{3}/2} & e^{ikb\sqrt{3}/2} & e^{ikb} & 0 & 0 \\ 0 & e^{-ikb\sqrt{3}/2} & e^{ikb\sqrt{3}/2} & 0 & e^{ikb} \\ 0 & 0 & e^{-ikb\sqrt{3}/2} & e^{ikb} & e^{ikb\sqrt{3}/2} \\ 0 & 0 & 0 & e^{ikb\sqrt{3}/2} & e^{-ikb\sqrt{3}/2} \end{pmatrix} \quad (25)$$

And $H_{BA}^{<2,1>} = H_{BA}^{<2,1>*}$. The electronic dispersion curves for this GNR are shown in figure 6(b). Note that the linear Dirac-like band structure has re-emerged for this ribbon. One third of AC-GNRs have Dirac sub bands, with the condition being $p + 1 \in 3N$ where N denotes the integers.

A typical ZZ-GNR band structure is shown in figure 6(a). The low energy band structure is no longer linear in this case, and all zig-zag ribbons have a zero-energy gap at the Fermi energy. This zero-gap condition is met over an extended region, which implies a very high density of states at the Fermi level. By selecting the appropriate width and chirality, a ribbon can be chosen with the desired electronic properties. One last example is shown in figure 6(c), which is the band structure of the <3,3> chiral ribbon. Note that this too has a low energy Dirac sub band structure. This is not the norm, and there are only a handful of cases where this is true for q > 1.

Vol. 13, Sp. Issue 03 July: 2025
ISSN(P) 2347-5404 ISSN(O)2320 771X

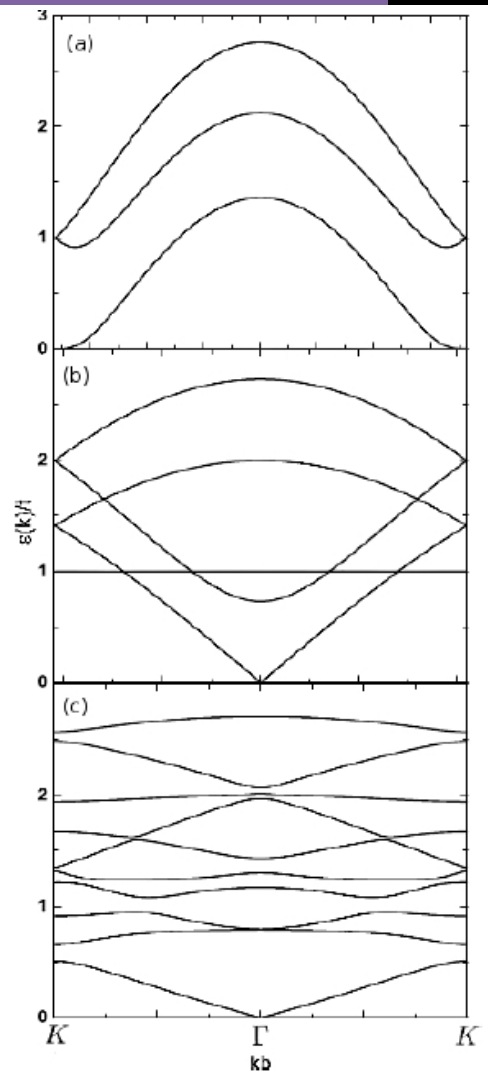

Figure 6 (a): A typical zig-zag nanoribbon band structure ($p = 2$). Note that at the brillouin zone edges the energy gap becomes zero. This is the case for all ZZ-GNRs. The linear Dirac dispersion is, however, not present, in these structures. (b) A typical armchair nonoribbon band structurer ($p = 2$). The low energy linear Dirac dispersion occurs in armchair ribbons where $p + 1 \subset N$. For all other AC-GNRs, there is a small band gap. (c) A $\langle 3, 3 \rangle$ chiral GNR. A small number of GNRs with $q > 1$ have a linear Dirac-like dispersion with no energy gap, but in general this will not be the case, and the bandgaps and curvature of the bands will vary dramatically from ribbon to ribbon.

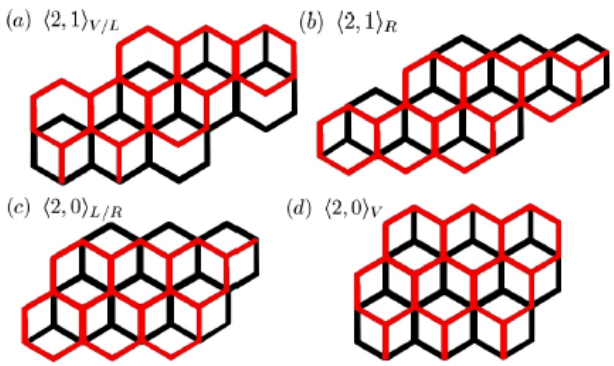

Figure 7 A selection of armchair and zig-zag lgnrs with the two distinct possible stacking orientations. These cause different edge sites to couple between layers in slightly different ways, leading to subtle changes in the electronic band structure.

7. Bilayer Graphene Nanoribbons (BLGNRs)

When constructing bilayer graphene using the normal 'bernal' type staking, the second is shifted along one of the three C-C lattice vectors relative to the first. The choice as to which lattice vector the shift is to be made along, in 2D bilayer graphene, is arbitrary, since a simple rotation of the entire system by an amount $2\pi/3$ or $4\pi/3$ will obtain the alternative orientations.

When constructing bilayer graphene nanoribbons however, the choice of lattice vector along which to shift the second layer alters the electronic properties of the ribbon in various ways. Due to the C3 symmetry of single layer graphene's hexagonal lattice, there are three equivalent ways to cut out any particular chirality ribbon. For example, cutting parallel to any of the three lattice vectors will produce an armchair ribbon, and cutting perpendicular to any lattice vector will produce a zig-zag ribbon.

With the second layer of bilayer graphene being shifted along one of the three lattice vectors however, this creates, in general, three inequivalent ribbon cuts. The C3 symmetry in this case, has been lost.

In the case of ZZ-and AC-BLGNRs however, due to their particular symmetry, there are only two inequivalent ribbons. Consider a second layer shift along $\hat{\delta}_1$ for example as in figure 7. When constructing an armchair bilayer ribbon out of this system, if the cut of parallel to $\hat{\delta}_2$, then flipping the system over (or viewing it from behind) will transform the ribbon to one cut parallel to $\hat{\delta}_3$. This is due to the equivalence of the two layers, meaning which one is the top layer and which one is the lower layer, in this case, is arbitrary. Similarly, consider a zig-zag ribbon cut out of the same system. If the cut is made perpendicular to $\hat{\delta}_2$, and then the system is flipped (or viewed from behind), it will appear to have been cut perpendicular to $\hat{\delta}_3$.

The high symmetry of these particular cases aside however, there are, in general, three inequivalent ribbons, of equal chirality, which can be cut out of bilayer graphene.
Including only the directly vertical interlayer coupling terms, one can determine the tight binding matrix elements from the Hamiltonian.

$$H = \sum_{i,j,l} t_{ij} c_{i,l}^{\dagger} C_{j,l} + \sum_{i,j} \gamma_{ij} c_{i,l_1}^{\dagger} C_{j,l_2} \quad (26)$$

Where i and j denote the lattice sites on layer l_1 or l_2, $t_{i,j} = t = 3.0\text{eV}$ is the regular intralyar nearest neighbor overlap matrix if i and j are nearest neighbors, and zero otherwise, and $\gamma_{ij} = \gamma = 0.13\text{eV}$ is the regular dominant interlayer term for bilayer graphene if i on l_1 is directly above j on l_2, and zero otherwise.
Returning to the case of the $\langle 2, 1\rangle$ ribbon, the Hamiltonian matrix is

$$H_{(2,1)}^{BLGNR} = \begin{pmatrix} H_{(2,1)}^{GNR} & H_{inter}^{S} \\ H_{inter}^{S} & H_{(2,1)}^{GNR} \end{pmatrix} (27)$$

Where S denotes the shift type : (V)ertical, (R)ight, or (L)eft. The vertical and left shift interlayer coupling matrices are equivalent in the armchair case, and are given by

$$H_{inter}^{V/L} = \begin{pmatrix} 0 & h_{V/L} \\ h_{V/L}^{T} & 0 \end{pmatrix} (28)$$

Vol. 13, Sp. Issue 03 July: 2025
ISSN(P) 2347-5404 ISSN(O)2320 771X

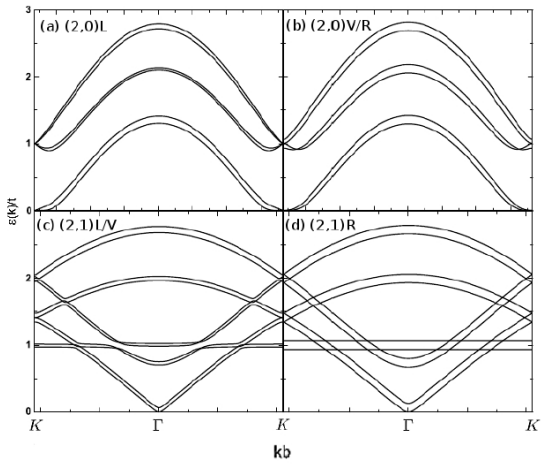

Figure 8: The band structurers for the high symmetry bilayer ribbons (q = 0,1)m with p = 2. In general, when going from a single to a bilayer ribbon, each single layer sub band becomes a sub band pair which are separated from each other by some amount determined by the interlayer edge state coupling. Note in particular the key differences depending on stacking orientation are at the K and Γ points.

Where

$$h_R = \begin{pmatrix} \gamma & 0 & 0 & 0 & 0 \\ 0 & \gamma & 0 & 0 & 0 \\ 0 & 0 & \gamma & 0 & 0 \\ 0 & 0 & 0 & 0 & \gamma \\ 0 & 0 & 0 & \gamma & 0 \end{pmatrix} \quad (29)$$

Is the right shift interlayer coupling matrix, and the vertical/left shift interlayer coupling matrix is given by

$$h_{V/L} = \begin{pmatrix} 0 & \gamma & 0 & 0 & 0 \\ 0 & 0 & \gamma & 0 & 0 \\ 0 & 0 & 0 & \gamma & 0 \\ 0 & 0 & 0 & 0 & 0 \\ 0 & 0 & 0 & 0 & \gamma \end{pmatrix} \quad (30)$$

The two inequivalent shifts of the second graphene layer in armchair nanoribbons are parallel to the axis direction, and at an angle of π/3 to the axis direction. The former leads to complete coupling of potentially vertical sites. This unique situation in armchair ribbons causes the band structure to two simple sets of curves with the simple form

$$\epsilon_i^{BLGNR} = \pm i\gamma + \epsilon^{SLGNR} \quad (31)$$

Where i = [0, 1]. This means that the bilayer armchair GNR with a parallel shift of the second layer has a set of curves equal of the single layer armchair ribbon, and a set of curves equal to the single layer ribbon but γ larger in magnitude.

The second type of bilayer armchair ribbon has some uncoupled sites in the unit cell which effects the bandgaps, making them, in general < γ, and not constant. Of particular interest are the low energy parts which are no longer two linear bands but instead curved as in 2D bilayer graphene, and at the usually degenerate points at |ϵ| = t, the points are no longer degenerate but a finite gap has emerged.

ZZ-BLGNRs are constructed the same way, except that the right and left shifts are equivalent in this case. The two inequivalent shifts of the second graphene layer in zig-zag nanoribbons are perpendicular to the axis direction, and at an angle of π/6 to the axis direction. The former leads to an entire overhanging edge on each layer which is not coupled to the other. This in turn leads to a larger deviation from the single layer electronic dispersion. The latter causes less sites to be uncoupled between layers, and so a less drastic shift form for the regular zig-zagribbon dispersion.

These single to bilayer and stacking dependent properties of the electronic dispersions of armchair and zig-zag bilayer nanoribbons can be seen in figure 8. When extending the system to three or more layers, the electronic properties evolve in the same way, and there are many distinct stacking orientations, as the different permutations and not, in general, equivalent.

However, we will not be particularly interested in these various stacking orientations in general. The results obtained for the vertical shift contains all the significant physics for this thesis, and from now on, it will be assumed that all BLGNRs are vertically shifted ones.

8. Conclusion

We can see from these results that the electronic properties of graphene-based materials vary significantly depending on dimensionality, layering and chirality. We see that single layer graphene is a zero-gap semiconductor. It stands in stark contrast to normal metals which exhibit diffusive electron transport and temperature dependent resistivity. The prediction and observation of a minimum dc conductivity and a universal ac conductivity stand as testament to these unique properties. In fact, graphene seems to be increasingly referred to as a super fluid rather than any kind of 'normal' electronic system. This seems sensible, as localization in suppressed, and so graphene is not highly correlated. It behaves more like a dilute gas in this respect. The Klein effect [19] makes the transport of Dirac Fermions [20] extremely robust to disorder, aiding the dissipation less transport expected of superfluids [21-24]. Band structure effects play the key role in all of these phenomena. Graphene is truly a unique material [4-6] with such varied properties that categorization into any conventional nomenclature is fruitless.

The derivation of the low energy Dirac Hamiltonian for single layer graphene has been nothing short of a phenomenon in condensed matter physics in the last few years. The Fermi energy in intrinsic graphene happens to lie precisely on the bands-touching points. This is a very interesting feature of graphene as it means that at the Fermi energy there is a vanishing density of states, and no bandgap. It is worth mentioning that the low energy bilayer Hamiltonian, whose form has not been considered as it is not relevant to this thesis, can essentially be described by the Dirac Hamiltonian with a mass term [6].

The chirality of graphene nanoribbons in particular promises some very exciting potential building blocks for electronic device implementation due to their chirality dependent band gaps. In particular, one can imagine that two ribbons, one armchair with zero-bandgap, and one chiral with a small finite band gap, can by joined together by simply cutting along one direction, then cutting along the other. And so semiconductor-metal junctions [25-27] can possibly be formed by simply cutting graphene along different directions. The holy grail in this context would be electronic device [28-37] production on the smallest scale ever achieved, by simply stamping out patterned graphene into networks of various chirality graphene nanoribons.

The main characteristic energies of layered graphene materials in particular lie within the terahetz to far infrared regime. The second nearest neighbour intralayer coupling, as well as all three major interlayer couplings are all within this region of the spectrum. Because of this, it is not unreasonable to expect that grapheme will be quite active within this region.

References

1. Block, F. (1928). Die metallische Faserstruktur der Metalle. *Journal of Physics*, 52, 555-580.
2. Boyle, W. S., & Nozières, P. (1958). Theory of electronic structure in graphite. *Physical Review*, 111(3), 782-790. https://doi.org/10.1103/PhysRev.111.782
3. Dillon, R. O., Spain, I. L., & McClure, J. W. (1977). Electronic band structure of graphite. *Journal of Physics and Chemistry of Solids*, 38(4), 365-374. https://doi.org/10.1016/0022-3697(77)90229-4
4. Ezawa, M. (2006). Graphene: From basic properties to novel applications. *Physical Review B*, 73(4), 045432. https://doi.org/10.1103/PhysRevB.73.045432

5. Geim, A. (2009). Graphene: Status and prospects. *Science*, 324(5934), 1530-1534. https://doi.org/10.1126/science.1158877
6. Geim, A., & Novoselov, K. (2007). The rise of graphene. *Nature Materials*, 6(3), 183-191. https://doi.org/10.1038/nmat1849
7. Hohenberg, P., & Kohn, W. (1964). Inhomogeneous electron gas. *Physical Review*, 136(3), B864-B871. https://doi.org/10.1103/PhysRev.136.B864
8. Klein, O., & Nishina, Y. (1929). The scattering of light by light. *Zeitschrift für Physik*, 52(11-12), 853-869. https://doi.org/10.1007/BF01345327
9. Kresse, G., & Furthmüller, J. (1996). Efficiency of ab-initio total energy calculations for metals and semiconductors using a plane-wave basis set. *Physical Review B*, 54(16), 11169-11186. https://doi.org/10.1103/PhysRevB.54.11169
10. Kresse, G., & Furthmüller, J. (1996). Efficient iterative schemes for ab initio total-energy calculations using a plane-wave basis set. *Computational Materials Science*, 6(1), 15-50. https://doi.org/10.1016/0927-0256(96)00008-0
11. Kresse, G., & Hafner, J. (1993). Ab initio molecular dynamics for liquid metals. *Physical Review B*, 47(1), R558. https://doi.org/10.1103/PhysRevB.47.R558
12. McClure, J. W. (1957). Band structure of graphite. *Physical Review*, 108(3), 612-618. https://doi.org/10.1103/PhysRev.108.612
13. Neto, A. C., Guinea, F., Peres, N., Novoselov, K., & Geim, A. (2009). The electronic properties of graphene. *Reviews of Modern Physics*, 81(1), 109-162. https://doi.org/10.1103/RevModPhys.81.109
14. Novoselov, K. et al. (2004). Electric field effect in atomically thin carbon films. *Science*, 306(5696), 666-669. https://doi.org/10.1126/science.1102896
15. Slonczewski, J. C., & Weiss, P. R. (1958). Band structure of graphite. *Physical Review*, 109(1), 272-279. https://doi.org/10.1103/PhysRev.109.272
16. Soule, D. E., McClure, J. W., & Smith, L. B. (1964). Electron states in graphite. *Physical Review*, 134(3), A453-A461. https://doi.org/10.1103/PhysRev.134.A453
17. Spry, W. J., & Scherer, P. M. (1960). Effect of pressure on the electronic properties of graphite. *Physical Review*, 120(4), 826-832. https://doi.org/10.1103/PhysRev.120.826
18. Wallace, P. R. (1947). The band theory of graphite. *Physical Review*, 71(9), 622-634. https://doi.org/10.1103/PhysRev.71.622
19. Williamson, S. J., Foner, S., & Dresselhaus, M. S. (1965). Magnetic susceptibility of graphite. *Physical Review*, 140(3), A1429-A1439. https://doi.org/10.1103/PhysRev.140.A1429